Supplemental Figures

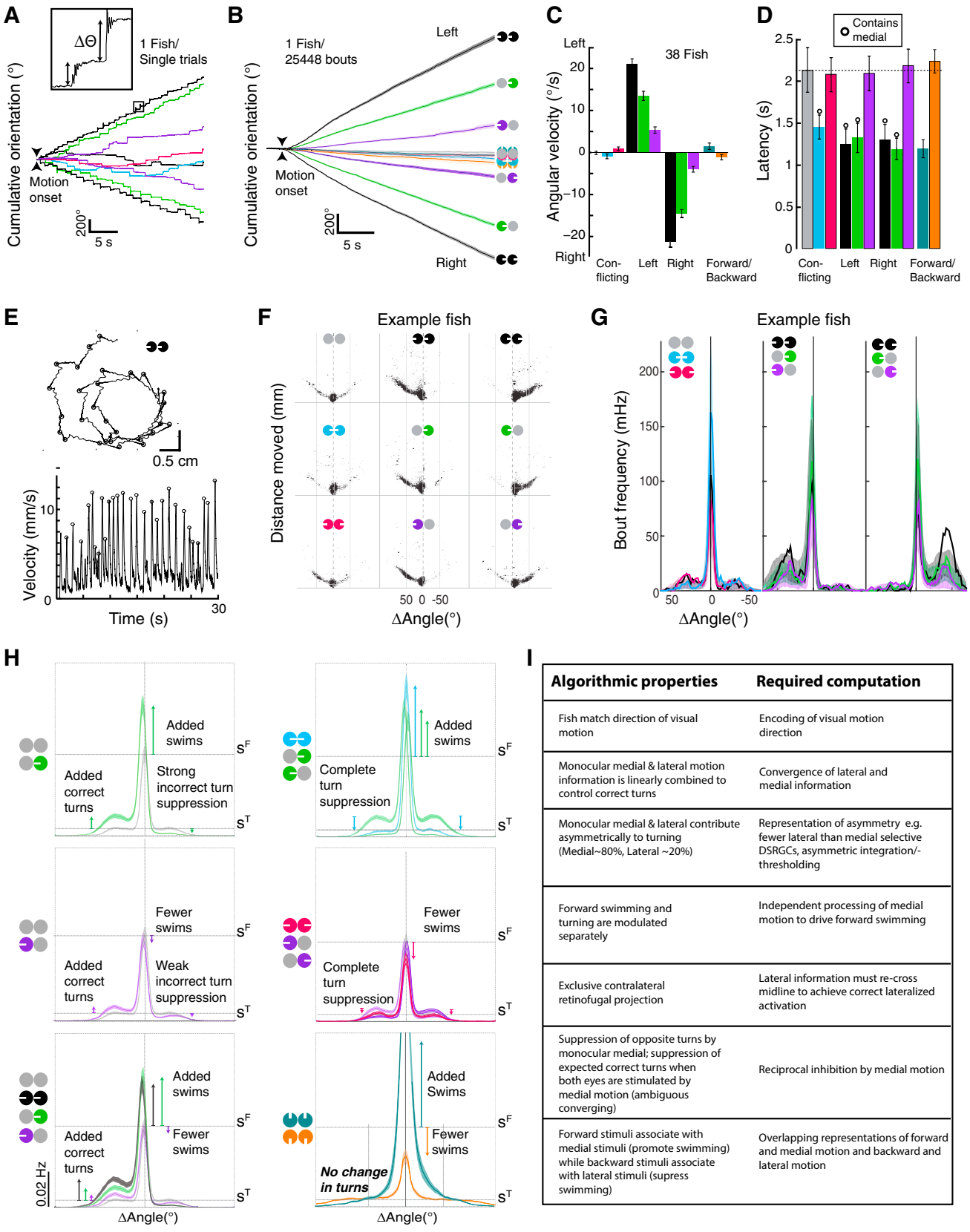

I

Algorithmic properties	Required computation
Fish match direction of visual motion	Encoding of visual motion direction
Monocular medial & lateral motion information is linearly combined to control correct turns	Convergence of lateral and medial information
Monocular medial & lateral contribute asymmetrically to turning (Medial~80%, Lateral ~20%)	Representation of asymmetry e.g. fewer lateral than medial selective DSRGCs, asymmetric integration/-thresholding
Forward swimming and turning are modulated separately	Independent processing of medial motion to drive forward swimming
Exclusive contralateral retinofugal projection	Lateral information must re-cross midline to achieve correct lateralized activation
Suppression of opposite turns by monocular medial; suppression of expected correct turns when both eyes are stimulated by medial motion (ambiguous converging)	Reciprocal inhibition by medial motion
Forward stimuli associate with medial stimuli (promote swimming) while backward stimuli associate with lateral stimuli (supress swimming)	Overlapping representations of forward and medial motion and backward and lateral motion

(legend on next page)

Figure S1. Behavioral Kinematics Necessitate Distinct Features of Underlying Neural Circuitry, Related to Figure 1

(A) Example trials of fish heading direction (orientation) change over time during presentation of the full stimulus set. Traces are aligned to the onset of visual motion (black arrowheads), with colors as in panel (B) and Figure 1B. Enlarged trace shows the orientation change ($\Delta\Theta$) for two individual swim bouts from boxed region. Note that fish behavior is characterized by periods of activity (turning or swimming) and periods of inactivity.

(B) Mean cumulative orientation change over time for a single zebrafish in response to the full stimulus set, as indicated by the icons to the right. Note that conflicting (inward and outward) and symmetric (forward and backward) stimuli produced no net orientation change, similar to the static control response. Shaded error is SEM across trials, n = 117 – 156 trials.

(C) Bar graph of average fish angular velocity (orientation change per second) to the full stimulus set, colors and icons as in (B). Baseline angular velocity was subtracted for each fish. Error bars are SEM across N = 38 fish.

(D) Bar graph of average latency to bout initiation after motion onset, colors and icons as in (B). Stimuli containing medial or forward motion information (open circles) evoked responses faster than any lateral or backward stimulus. Dotted line signifies the average latency for the static condition. Error bars represent SEM across N = 38 fish.

(E) *Top*, x-y trajectory of a single fish during a single trial (30 s) in which the fish was presented with binocular leftward motion. Fish responded with discrete, consecutive bouts (open black circles) oriented to the left. *Below*, a velocity plot of the same trial illustrates the bout structure of the behavior, which allowed for detection of single locomotion events (open circles).

(F) Scatterplots of distance and orientation change (Δ Angle) for extracted bouts during presentation of the full stimulus set (N = 1 fish, n = 24,558 bouts, 117 – 156 stimulus repetitions, 11.8 hr). Each bout is plotted as a black point, illustrating the distance moved and angle change for each locomotion event. Note the symmetric distribution of right and left bouts for static, conflicting outward (magenta), and conflicting inward (blue). In contrast, stimuli with net motion (coherent, monocular medial, and monocular lateral) caused behavioral biases in the direction of motion (left for leftward stimuli, right for rightward stimuli). Note how stimuli containing a medial stimulus evoked bouts with larger distances and biased forward swims. While lateral motion stimuli evoked turns in the correct direction (following the direction of motion), incorrect turns (opposite the direction of motion) were still permitted. Colors and icons as in Figure 1B.

(G) Histogram of bout angles for a single fish, plotted on top of mean ± standard deviation (shaded area) across all fish.

(H) Annotated average bout frequency histograms for each stimulus. Each panel illustrates the effect of motion on behavioral output. Colors and icons as in Figure 1B. "Swims" refer to the central forward swimming peaks. Accompanying arrows denote the direction and magnitude of each highlighted effect. s^F, baseline forward swimming frequency during the static condition; s^T, baseline turning frequency during the static condition.

(I) Table of behavioral observations (algorithmic properties) matched with hypothesized neural computations.

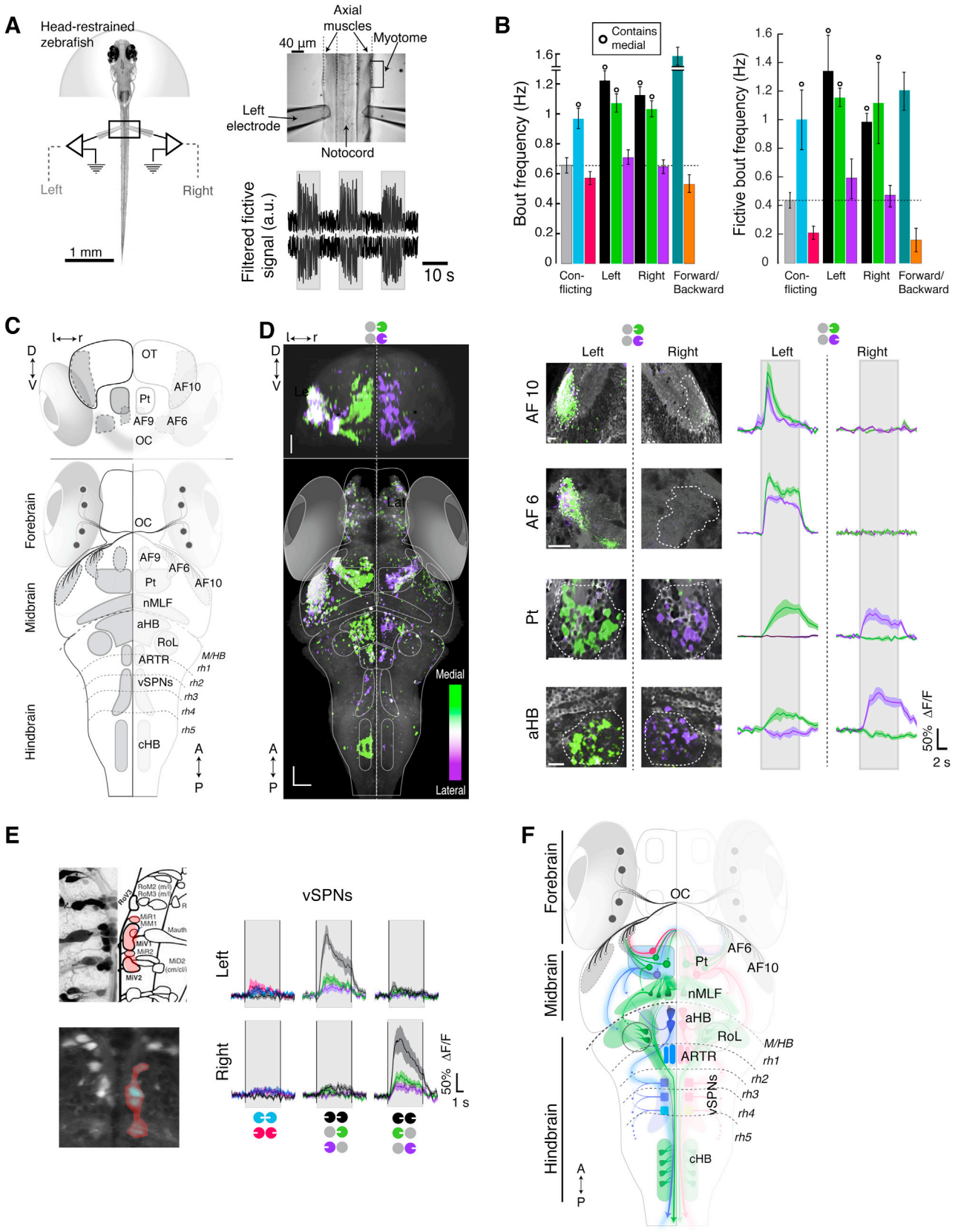

(legend on next page)

Figure S2. Fictive Locomotion Patterns and Identification of Optic Flow Processing Centers with Whole-Brain Imaging, Related to Figure 2

(A) Schematic of paralyzed, head-restrained larval zebrafish with fictive recording electrodes measuring intended locomotion via peripheral motor nerve electrophysiology. *Right top*, transmission image of electrode configuration. *Right bottom*, example traces of fictive recordings from the left (*top*) and right (*bottom*) electrodes during presentation of whole field leftward motion. Three stimulus repetitions (gray) are shown with intermittent baseline periods, concatenated.

(B) *Left,* average freely swimming bout frequency (N = 38 fish) during presentation of the full stimulus set. Stimuli containing medial or forward motion (open circles) increased bout frequency above baseline (during static condition, gray dotted line). Bars are color-coded as in Figure 1B. *Right,* average fictive bout frequency (N = 3 fish, see STAR Methods) during presentation of the full stimulus set. The general pattern of visually evoked bout frequency modulation was comparable to freely moving fish. Error bars represent SEM across fish.

(C) Schematic reference drawing of frontal (top) and dorsal (bottom) views of the larval zebrafish brain. A, anterior; P, posterior; D, dorsal; V, ventral; l, left; r, right. Anatomical outlines show the locations of relevant brain regions that process motion information. Pt, pretectum; OC, optic chiasm; OT, optic tectum; AF6, 9, 10, retinal arborization fields 6, 9, 10; nMLF, nucleus of the medial longitudinal fasciculus; vSPNs, ventromedial spinal projection neurons; ARTR, anterior rhombencephalic turning region; aHB, anterior hindbrain; RoL, neurons in rhombomere 1; cHB, caudal hindbrain; M/HB, midbrain-hindbrain border (dashed line); rh1-5, rhombomeres 1-5.

(D) *Left*, monocular whole-brain activity map generated by sequential presentation of monocular lateral and monocular medial motion to the right eye (see icons on top). Pixels are colored if their activity was significantly correlated with either monocular medial or lateral stimulus presentation. Pixels more correlated with medial are green, and pixels more correlated with lateral are purple. Regions that responded to both directions of motion appear white (see colorbar). The map is a maximum intensity projection through 135 μm of tissue, with ventral AF10 as the most dorsal plane. Note that signals converged in AF6 and AF10 but diverged in the Pt. Scale bar, 50 μm. *Right*, single planes showing activation in AF10, AF6, Pt, and aHB. Adjacent, average ΔF/F traces of the indicated ROIs (dashed white lines). Scale bars, 10 μm. Shaded areas represent SEM over 10 stimulus repetitions.

(E) *Top left*, schematic of spinal projection neuron morphology in the zebrafish hindbrain (adapted from Orger et al., 2008), with vSPNs highlighted in red. *Right*, average ΔF/F traces for left and right vSPNs backfilled with Oregon Green BAPTA-488 (*bottom left*). vSPNs showed strong direction selectivity and binocular activation, with minimal responses to conflicting motion. Colors and icons as in Figure 1B. Gray bars are stimulus presentation periods. *Left*, N = 7 fish. *Right*, N = 9 fish. Shaded areas represent SEM across fish.

(F) Whole-brain, map-derived model of information flow for the zebrafish OMR. DSRGCs in the retina (gray circles) send motion streams to contralateral AF6 and AF10. Moving from anterior to posterior, the left Pt, which exhibits the binocularity predicted from behavior, then collects leftward (blue) and forward (green) motion signals, and the right Pt collects rightward (red) and forward (green) motion signals. Anatomically distinct regions in the hindbrain (cHB, RoL) and midbrain (nMLF) are highly forward-selective activity and may thus influence forward swimming. Other regions in the hindbrain (aHB, ARTR, vSPNs) show strong tuning to either leftward or rightward motion and may thus influence turning. The nMLF and vSPN regions contain spinal projection neurons (descending arrows) that are known to directly affect behavior. M/HB, midbrain-hindbrain border (dotted line). rh1-5, rhombomeres 1-5.

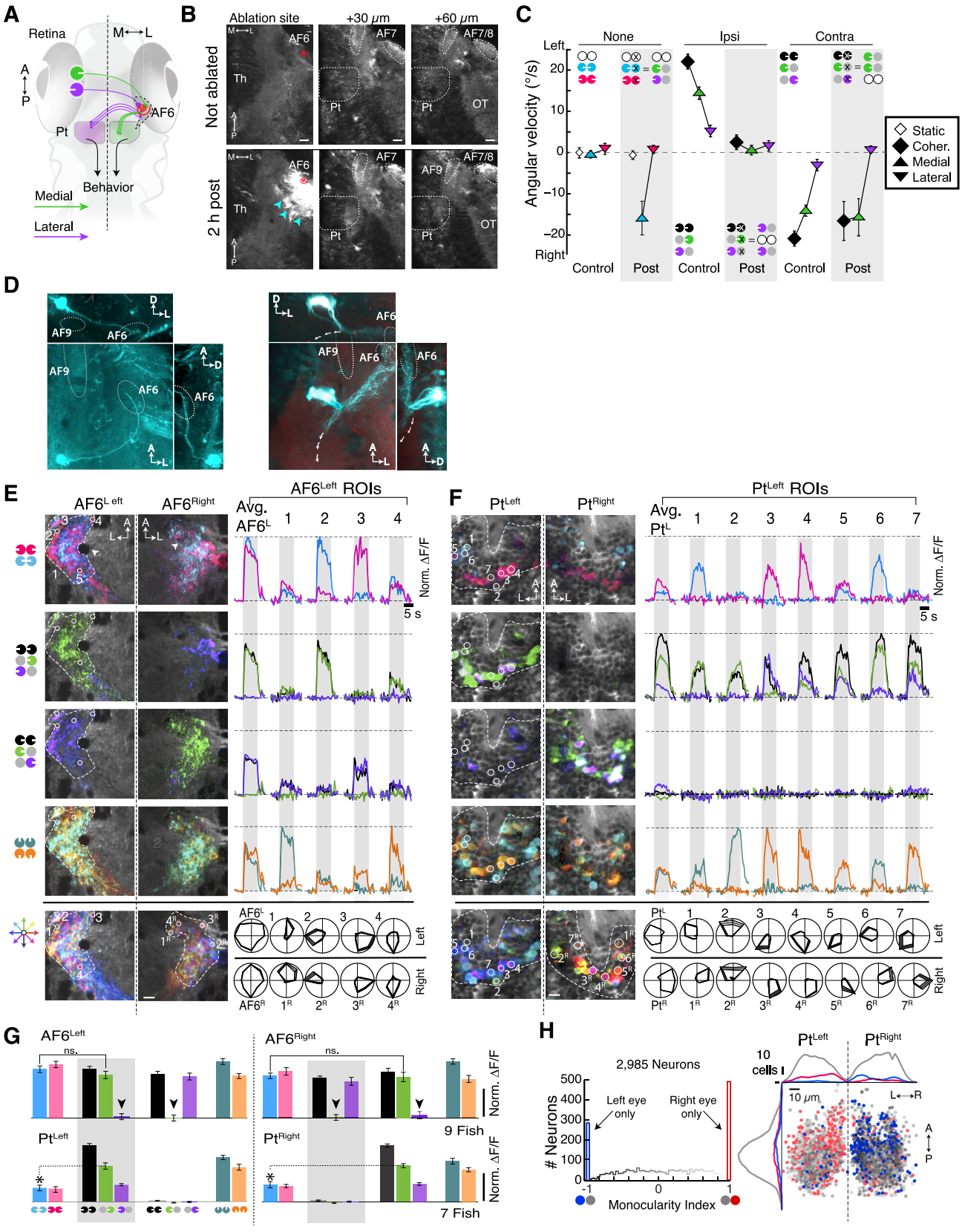

(legend on next page)

Figure S3. Laser Ablations, Anatomical Tracing, and Ca^{2+}-Imaging Demonstrate the Role of AF6 and Pt in Optic Flow Processing, Related to Figure 2

(A) Schematic illustrating a unilateral laser ablation of AF6 and its expected effect on behavior. If AF6 is the main entry site for OMR-relevant motion information, AF6 lesions (red spiral) should lead to disruption of behavior normally evoked by stimulation of the contralateral eye. M, medial; L, lateral; A, anterior; P, posterior.

(B) Example of AF6 laser ablation in a *Tg(elavl3-GCaMP2)* fish across 3 imaging planes. Damage (blue arrow heads, *bottom*) was observed surrounding the ablation site (red spiral). Th, thalamus; Pt, pretectum; OT, optic tectum. Scale bar, 10 μm.

(C) Average angular velocity (orientation change per second) in response to the stimulus set in control fish (N = 38) and fish after unilateral AF6 ablation (N = 8). Effects generally suggest that AF6 ablated fish behave as if stimulated in only one eye (symbols show how a given stimulus would look to the fish if no motion would be perceived through the eye associated with the ablated AF). After ablation, fish interpreted conflicting inward motion as monocular medial motion, and behavior appeared to be driven only by motion presented to the eye contralateral to the ablation site. Colors and icons as in Figure 1B. Error bars are SEM across fish.

(D) *Left*, PA-GFP imaging after photoactivating a single neuron in the Pt in a *Tg(α-tubulin:PA-GFP)* fish. Side and top view show neurites in AF6. *Right*, imaging a group of photoactivated direction-selective neurons in the Pt. Side and top view show projections into AF6 and dim ventrally descending projections (white arrows). A, anterior; D, dorsal; L, lateral.

(E) *Left*, two-photon micrographs showing anatomy (gray) and average ΔF/F activity (colors) in the left and right AF6 ($AF6^{Left}$ and $AF6^{Right}$, respectively) for a representative fish. Stimulus icons as in Figure 1B, with activity is color-coded accordingly. *Right*, trial-averaged ΔF/F time series for the entire $AF6^{Left}$ and indicated subROIs. The spatial extent of these regions roughly matched the size of synaptic boutons (< 1 um^2), reinforcing the idea that AF6 activity represents direct preprocessed motion signals from retinal axons. To emphasize relative differences in activity across stimuli, the ΔF/F for each ROI was normalized to its maximum response across the stimulus set (horizontal dotted lines). Gray bars represent stimulus presentation periods. *Bottom*, responses to 8 whole-field motion stimuli. Here, active pixels are colored according to preferred motion direction (see color wheel). Polar plots for indicated ROIs show mean normalized ΔF/F ± SEM across trials in response to each motion direction. Note that AF6 was exclusively monocular and contained all directional information.

(F) *Left*, two-photon micrographs showing anatomy (gray) and average ΔF/F activity (colors) in the left and right Pt (Pt^{Left} and Pt^{Right}, respectively) for a representative fish (color-coded as in (E). *Right*, trial-averaged ΔF/F time series for the entire Pt^{Left} and indicated subROIs. To emphasize relative differences in activity across stimuli, the ΔF/F for each ROI was normalized to its maximum response across the stimulus set (horizontal dotted lines). Gray bars represent stimulus presentation periods. *Bottom*, responses to 8 whole-field motion stimuli. Here, active pixels are colored according to preferred motion direction (see color wheel). Polar plots for indicated ROIs show mean normalized ΔF/F ± SEM across trials in response to each motion direction. Note that the Pt integrated motion information binocularly and showed sharp directional tuning.

(G) *Top left*, bar graphs of average normalized RGC terminal ΔF/F in $AF6^{Left}$ in response to each stimulus. *Top right*, responses for $AF6^{Right}$. N = 9 fish. Motion presented to the ipsilateral eye did not result in activation (black arrowheads), and there was no difference in activation between monocular medial stimuli and binocular coherent stimuli. *Bottom*, bar graphs of average normalized Pt ΔF/F for the Pt^{Left} and Pt^{Right} in response to the same stimulus set. Pt responses were segregated by motion direction, and showed binocular integration and inward suppression. N = 7 fish. Error bars are SEM across fish. (*) $p < 0.001$; (ns.) $p > 0.05$, paired Wilcoxon.

(H) *Left*, distribution of neurons in the Pt activated by the left eye only (blue), mostly left eye (darker), mostly right eye (lighter), or only by the right eye (red). *Right*, spatial distribution of Pt neurons, color-coded according to binocularity index. Histograms show the relative distribution along the anterior-posterior axis (*left*) and also left to right across the midline (*top*). Monocular neurons (red or blue) were located predominantly in the Pt contralateral to the respective stimulus.

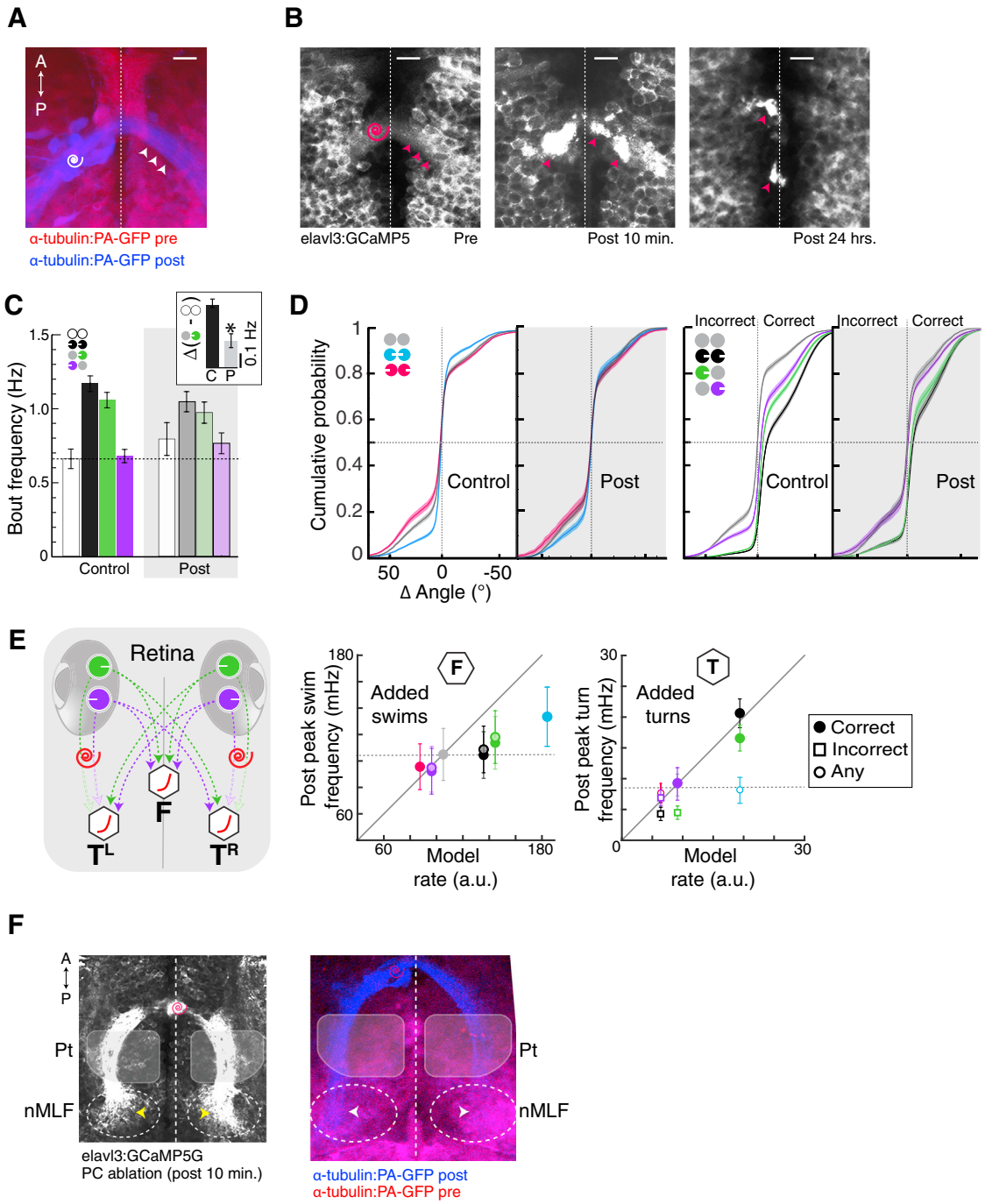

Figure S4. Ablation of Posterior Commissure Disrupts Interhemispheric Communication, Related to Figure 4

(A) Two-photon maximum intensity projection of the brain region containing the PC in a *Tg(α-tubulin:PA-GFP)* fish. Composite images show neural tissue before (red) and after (blue) photoactivation of a small region (white spiral). Unchanged areas appear magenta, while activated projections appear blue, revealing neuronal cell bodies ipsilateral to the activation and axonal tracks crossing the midline (white arrow heads). Dotted white line, fish midline. A, anterior; P, posterior. Scale bars, 10 μm.

(B) Two-photon micrographs showing the dorsal section of the PC before and after ablation in a 5 dpf *Tg(elavl3-GCaMP2)* fish. Red spiral, ablation site. Red arrowheads, neurites (Pre-ablation image) and debris (Post-ablation images).

(C) Bar graphs of average bout frequency show no significant differences after ablation (static control versus post-ablation, p = 0.33; coherent control versus post-ablation, p = 0.08, unpaired Wilcoxon). *Inset*, difference between average bout frequency for monocular medial stimuli and baseline (static condition) reveals a significant reduction in relative bout frequency after PC ablation. C, control; P, post-ablation. Bar colors match icons (*top left*) as in Figure 1B. Error bars are SEM across fish (N = 38 for control, N = 14 post-ablation). (*) p = 1.4×10^{-5}, unpaired Wilcoxon.

(legend continued on next page)

(D) Cumulative probability histograms of bout angle for control fish and fish post-PC ablation. The change in turn probability for coherent and monocular lateral motion indicates that commissure ablation disrupted correct turns generated by lateral motion stimuli.

(E) *Left*, schematic of minimal model in which DSRGCs drive turning (T) and forward swim motor command centers (F), without ipsilateral connections (spirals); this represents the hypothesized perturbation by PC ablation. *Middle*, comparison of measured peak swim frequency in ablated fish and model output without ipsilateral connections. Each point represents the mean peak response to a stimulus, with colors as in panel (D) and Figure 1B; lighter center indicates leftward motion. Error bars are SEM across fish. Although the model predicts no effect on swim frequency, the measured PC behavior indicated that medial-evoked swim frequency was affected by PC ablation. *Right*, the model can predict post-ablation peak turn frequencies well regarding the reduction of the lateral contribution to binocular integration (monocular lateral indistinguishable from baseline, coherent indistinguishable from monocular medial), but incorrectly predicts high turn frequencies in response to inward motion (blue circle). The model also fails to describe the persistence of incorrect turn suppression for coherent and monocular medial stimuli (black and green open squares). Dotted lines indicate static baseline rates.

(F) *Left*, PC ablation (at spiral) in an example *Tg(elavl3-GCaMP5G)* fish resulted in activation or injury of all passing axons. The concomitant increase in fluorescence can be used to visualize the axonal projections of Pt (gray boxed regions) neurons through the PC into nMLF (dotted ovals, yellow arrowheads). *Right*, this result agrees with data collected from PA-GFP fish after photoactivating a small region of the PC (spiral).

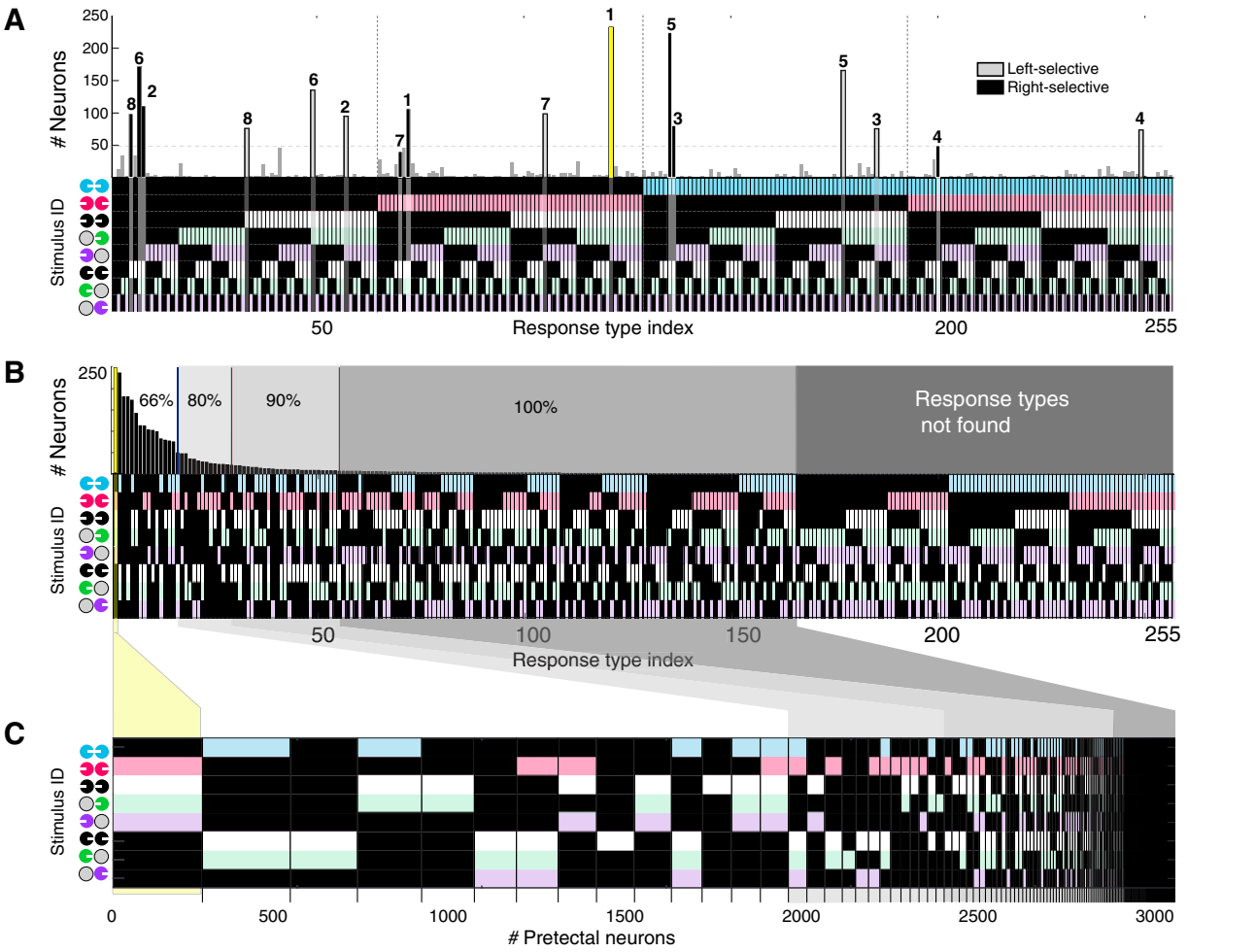

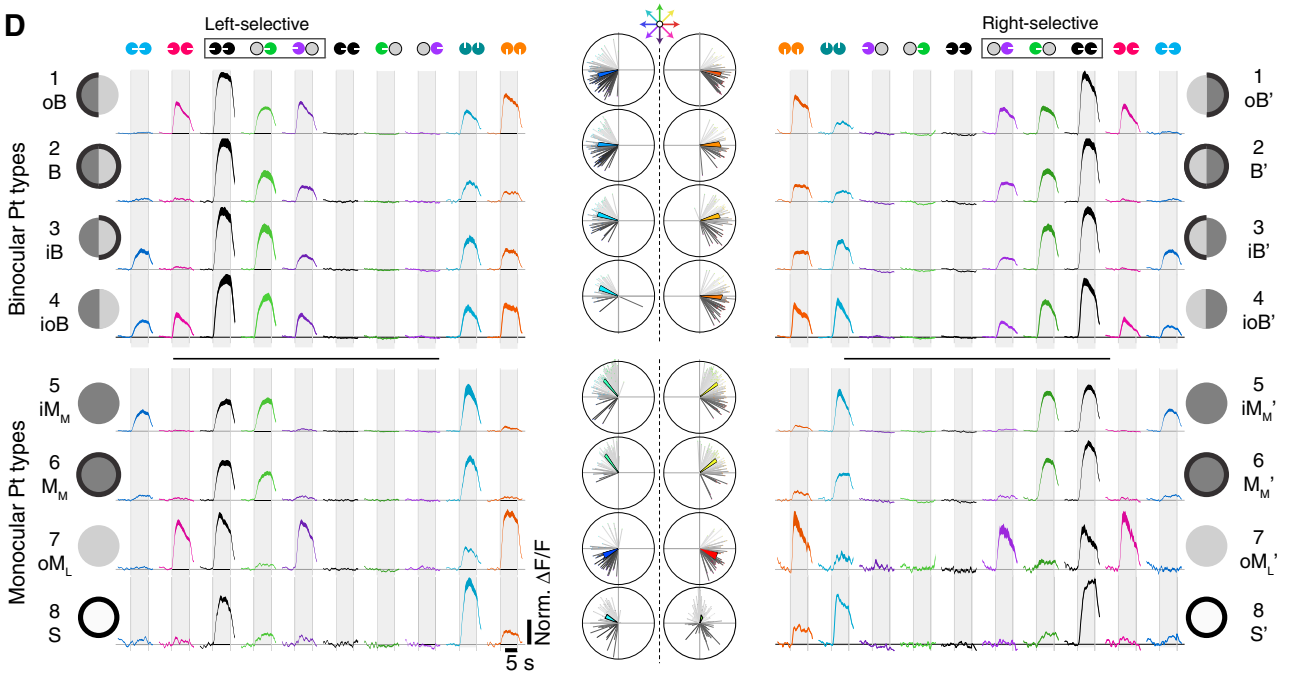

(legend on next page)

Figure S5. Functional Classification of Pretectal Neurons, Related to Figure 5

(A) Frequency of neuron response types, based on significant ΔF/F increases during presentation of monocular and binocular motion patterns (STAR Methods). *Top*, overrepresented types (numbered 1-8) are highlighted in gray (left-selective) or black (right-selective). All types below the dotted line have frequencies below the apparent discontinuity evident from sorted histograms in Figure 5C. *Bottom*, matrix representation of all possible response types, aligned with the plot above so that each column reveals a particular response pattern across the stimulus set. Combinatorial matrix represents significant responses (colored) and non-responses (black) to the stimulus indicated in each row, color-coded according to the stimulus icons to the *left*. Most frequent response type oB is highlighted in yellow.

(B) *Top*, sorted frequency histogram of neuronal response profiles, based on significant increases in GCaMP5 ΔF/F during presentation of motion stimuli (STAR Methods, Figure 5A). Bar corresponding to the most frequent response type (oB) is highlighted in yellow. The dip in neuronal frequency shows that the 8 most frequent response types (Figures 5A–5C) make up 66% of all neurons. Furthermore, only 188 response types of all possible categories are found. *Bottom*, associated sorted response matrix, aligned with the plot above so that each column reveals a particular response pattern across the stimulus set; combinatorial matrix represents significant responses (colored) and non-responses (black) to the stimulus indicated in each row, color-coded according to the icons on the left.

(C) The response type matrix from (A) but with the width of each column dictated by the share of neurons in each category. Response type oB is highlighted in yellow and now expanded.

(D) Average normalized ΔF/F in response to each stimulus for left-selective neurons (*left*), matched with the responses of their mirror symmetric counterparts (*right*), for each of the top 8 response types. Shaded areas are SEM across neurons in each category. Gray bars denote stimulus presentation periods. *Middle*, average (vector sum) direction selectivity vectors for each respective type along with vectors for each individual neuron in each category. oB, outward-responsive binocular neuron; B, binocular; iB, inward-responsive binocular; ioB, outward- and inward-responsive binocular; iM_M, inward-responsive monocular (medial-selective); M_M, monocular (medial-selective); oM_L, outward-responsive monocular (lateral-selective); S, selective for coherent motion. Rightward-selective types are indicated by (′). Each class is labeled according to its response profile, illustrated by adjacent circular icons; center, fraction of medial (dark gray) or lateral (light gray) activation; black outer ring, suppression by inward or outward motion. See symbol legend in Figure 7.

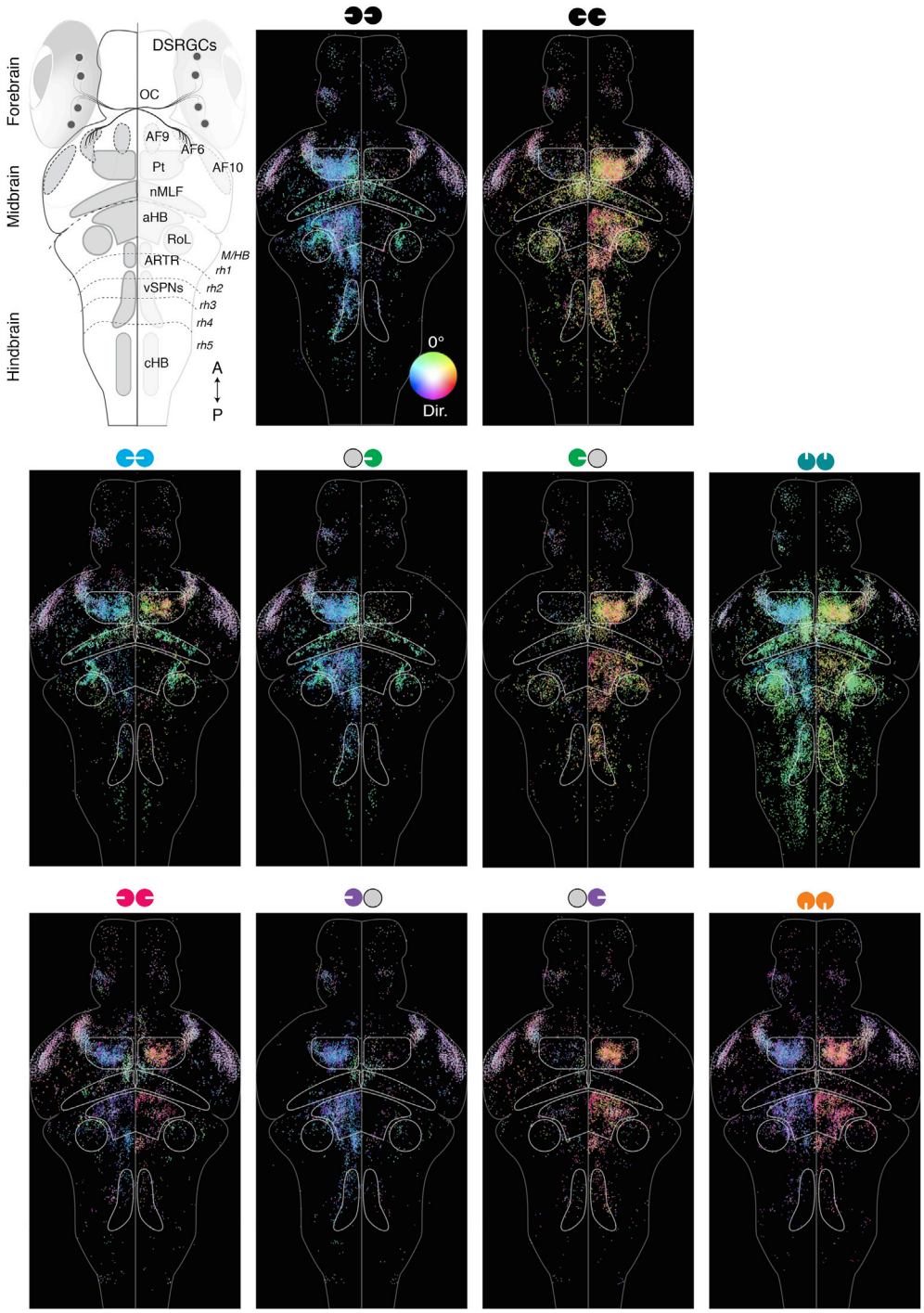

Figure S6. Brain-wide Recruitment of Turning- and Swimming-Related Neural Networks, Related to Figure 6

Top left, anatomy reference. DSRGCs, direction-selective retinal ganglion cells; OC, optic chiasm; AF6, 9, 10, retinal arborization fields 6, 9, 10; Pt, pretectum; nMLF, nucleus of the medial longitudinal fasciculus; aHB, anterior hindbrain; RoL, neurons in rhombomere 1; ARTR, anterior rhombencephalic turning region; vSPNs, ventromedial spinal projection neurons; cHB, caudal hindbrain; M/HB, midbrain-hindbrain border (dashed line); rh1-5, rhombomeres 1-5. A, anterior; P, posterior.

Other panels, anatomical distributions of units recruited during motion stimuli (icons as in Figure 1B). In total, n = 76,604 units isolated with automatic segmentation across 14 fish. Each unit is plotted on a standard brain map as single dot, 80% transparency, color-coded for preferred motion direction as in Figure 2B (see Dir. color wheel).

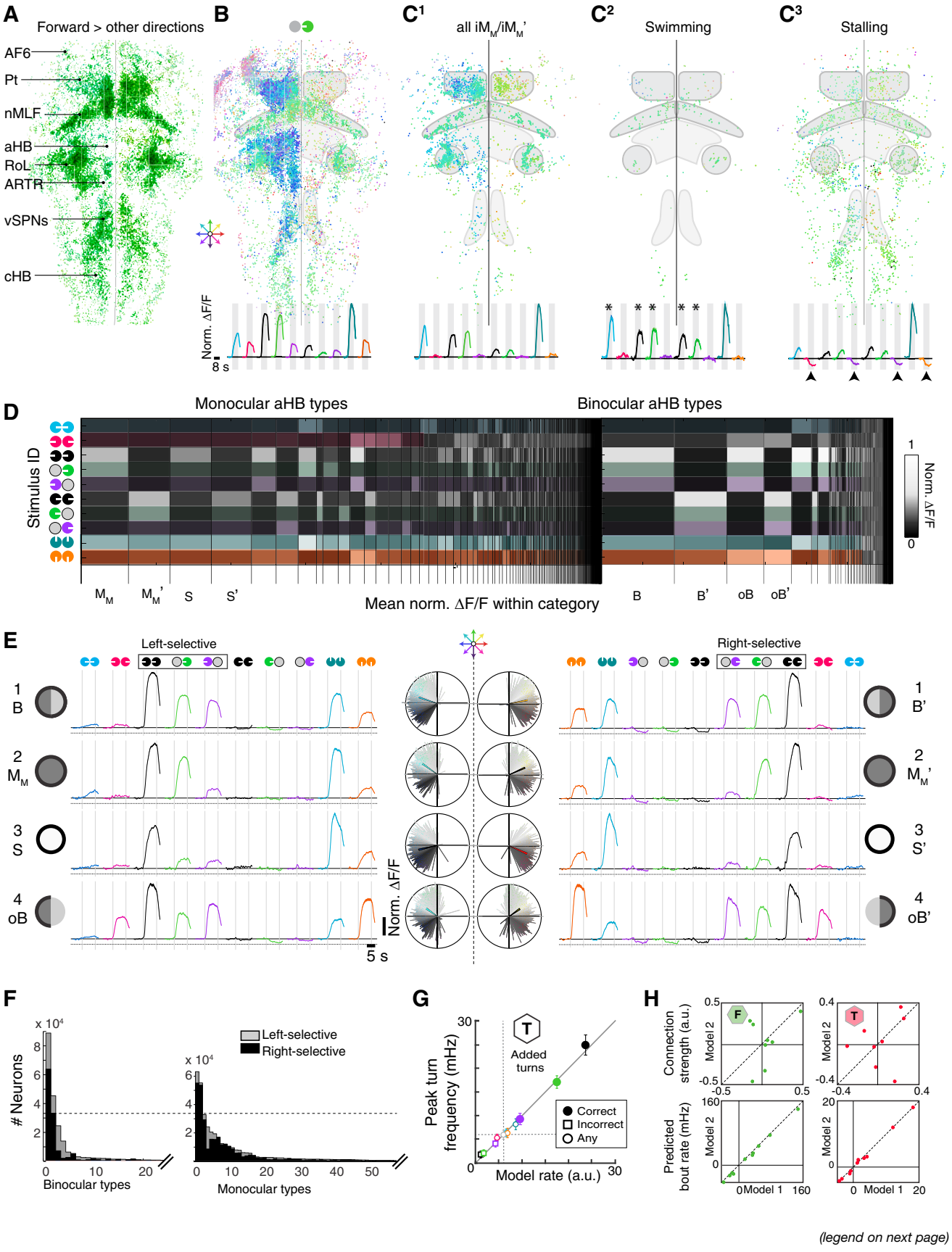

(legend on next page)

Figure S7. Analysis of Hindbrain Circuitry Supports Functional Whole-Brain Model, Related to Figures 6 and 7

(A) Distribution of units with higher peak ΔF/F responses to forward than the other 7 directions (42.5% of all motion sensitive units). Activity in these units is thus more associated with forward swimming than turning. Each unit is plotted on a standard brain map as a single dot, color-coded for preferred direction of motion (see color wheel). Regions with high unit density appear darker. AF6, arborization field 6; Pt, pretectum; nMLF, nucleus of the medial longitudinal fasciculus; aHB, anterior hindbrain; RoL, region in rhombomere 1; ARTR, anterior rhombencephalic turning region; vSPNs, ventral spinal projection neurons.

(B) Distribution of all units significantly activated by monocular medial regardless of their activation by other stimuli. Units are color-coded according to direction preference (see color wheel). Note the strong lateralization of neural recruitment in the left Pt and aHB (blue hues) and the symmetric recruitment of forward-selective units in nMLF, RoL, cHB (green hues). *Bottom*, mean normalized ΔF/F traces for all displayed units, color-code and stimulus sequence as in panel (D) and Figure 1B. A simplified mask is overlaid to compare anatomy to (A).

(C^1) Distribution of all units that are categorized as either iM_M (left-selective) or iM_M' (right-selective). These units are good candidates for the drive of forward swimming. Note units in nMLF, RoL. C^2 All iM_M units that show large responses to the stimuli marked with an asterisk (inward, coherent, monocular medial), which promote forward swimming. Note their clustering in nMLF and their high activation by forward motion. C^3 All units showing significant suppression below baseline for stimuli that suppress forward swimming (outward, monocular lateral, backward motion, arrowheads). Note their symmetric distribution in brain regions associated with forward swimming (nMLF, RoL, cHB). Below, mean normalized ΔF/F traces across all units displayed in each respective plot.

(D) Heatmap of mean normalized ΔF/F within monocular (*left*) and binocular (*right*) neuron response categories in the anterior hindbrain. Categories are based on significant ΔF/F increases during presentation of monocular and binocular motion patterns (STAR Methods). The width of each column corresponds to the frequency of each neuron type, the hue to stimulus icons on the *left*, and brightness to mean normalized ΔF/F within each category. Each type is labeled according to its response profile: oB, outward-responsive binocular neuron; B, binocular; M_M, monocular (medial-selective); S, selective for coherent motion.

(E) Average normalized ΔF/F in response to each stimulus for left-selective neurons (*left*), matched with the responses of their mirror symmetric counterparts (*right*), for the 4 over-represented aHB response types (numbers correspond to labels above bars in (D). *Middle*, average (vector sum) direction selectivity vectors for each respective type along with vectors for each individual neuron in each category. Each type is labeled according to its response profile, illustrated by adjacent icons; center, fraction of medial or lateral activation; black outer ring, suppression by inward or outward motion. See symbol legend in Figure 7G. Neuronal abbreviations as in (D).

(F) Sorted histograms of aHB response type frequency, plotted separately for binocular (*left*) and monocular (*right*) types. Major types have frequencies above the indicated discontinuity threshold (dotted line, see STAR Methods).

(G) Comparison of measured peak turn frequency with model including the hindbrain (cf. Figure 7A). repairs the prior deficiency in incorrect turn suppression (cf. Figure 5E). Each point represents the mean peak response to a stimulus, with colors as in panel Figure 1B.

(H) Diverse models can predict similar behavioral outputs. *Top*, comparison of two sets of connection weights to F (*left*, green) and two sets of connection weights to T (*right*, red). Each point represents a neuron type. *Bottom*, each set of connection weights effectively recapitulates the behavior. Each point represents the behavioral response to a stimulus (like in [G]).